Mater. Res. Soc. Symp. Proc. Vol. 1373 © 2012 Materials Research Society
DOI: 10.1557/opl.2012.288

Structure of Dislocations and Mechanical Properties of B2 Alloys

V. Paidar[1] and V. Vitek[2]
[1]Institute of Physics AS CR, Na Slovance 2, 182 21 Praha 8, Czech Republic
[2]Department of Materials Science and Engineering, University of Pennsylvania, 3231 Walnut Street, Philadelphia, PA 19104, U.S.A

ABSTRACT

Adequate mechanical properties are important for both structural and functional applications of materials. There are significant differences in mechanical behaviour of different B2 ordered alloys and these are related to the properties of superlattice dislocations. Several types of dislocations can be activated, in particular <111> and <001> dislocations gliding on {110} planes. Their mobility can vary markedly from material to material and this has a strong impact on the mechanical properties. With the aim to elucidate qualitatively the differences between different alloys crystallising in the same B2 structure we analyse possible dislocation dissociations. The model employed is based on the isotropic elasticity but includes an important characteristic of stacking-fault-like defects involved in the splittings, the deviation of their displacements away from the usually assumed ½<111> APB.

INTRODUCTION

Mechanical properties of B2 intermetallic compounds and alloys are controlled by the type of active dislocations. The shortest lattice vector in the B2 structure is <001> and therefore these dislocations are likely to possess the lowest energy. Hence, the <001> slip direction is expected to be dominant. There are, indeed, B2 alloys in which the principal slip direction is <001> (e. g. CoTi [1-3]) but the <111> slip dominates in others (e.g CuZn [4] or FeAl [5, 6]) in spite of the fact that the square of the <111> Burgers vector is three times larger than that of the <001> vector and, therefore, the energy of the <111> dislocations is expected to be much higher than that of <001> dislocations. However, the dislocation energy is not the only criterion determining which dislocations mediate the slip. Another factor, which may be even more important than the energy, is the dislocation mobility that depends crucially on the dislocation core structure [7], in particular on the ability of dislocations to split into partial dislocations separated by metastable stacking-fault-like defects. For example, if dislocations possess narrow non-planar cores their motion is restricted since these cores must be first transformed from their sessile form to a glissile form. The well-known example is BCC metals. On the other hand, dislocations with planar cores are usually quite mobile since their cores are already in the glissile form. The latter is usually the case if dislocations dissociate into a crystal plane like, for example, in FCC metals.

It is commonly accepted that in materials with metastable stacking faults that possess sufficiently low energies the dislocations dissociate into well-separated partials which renders dislocation cores planar. It has been generally assumed that in B2 ordered alloys the APB of the type ½<111> is a metastable fault on {101} planes and that its energy is related to the order-disorder transition temperature between the ordered B2 and disordered BCC phase. If this were the case then when the order-disorder transition temperature is low the APB energy is low and thus <111> superdislocations may dissociate into two well separated ½<111> superpartials and in this case the <111> slip direction will be favoured [8-10]. This appears to be the case in CuZn but for example CoTi and FeAl are both ordered up to the melting temperature and as a result

have very high transition temperatures but the <001> slip is dominant in the former while the <111> slip operates in the latter.

However, as found in a number of atomistic studies [11-16], the ½<111> APB may not be a metastable fault on {110} planes. Instead, displacements leading to metastable faults are not determined by crystallography but by details of atomic interactions and vary from material to material. Specifically, in the (110) plane the fault vector may be shifted away from $\frac{1}{2}[1\,\bar{1}\,1]$ along the $[1\,\bar{1}0]$ direction. The dislocations with the Burgers vector $\mathbf{b} = [1\,\bar{1}\,1]$ may then dissociate into three partials, as shown in Fig. 1,

$$\mathbf{b} = \mathbf{b_1} + \mathbf{b_2} + \mathbf{b_1}. \quad (1)$$

Similarly, the dislocation with the Burgers vector **a** = [001] may also dissociate following the reaction

$$\mathbf{a} = \mathbf{b_1} + \mathbf{b_3} \quad (2)$$

where $\mathbf{b_3}$ has the same magnitude as $\mathbf{b_1}$ but different direction (see Fig. 1).

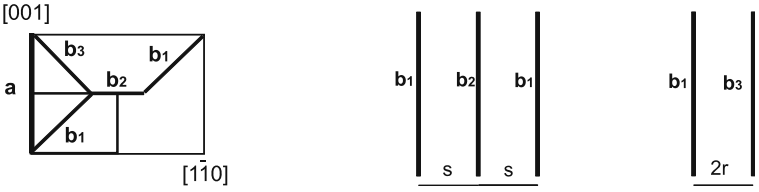

Figure 1. Dissociations of $[1\,\bar{1}\,1]$ and [001] dislocations on the (110) plane in a B2 lattice according to equations (1) and (2), respectively.

Figure 2. Definition of the widths of splittings for the $[1\,\bar{1}\,1]$ dislocation dissociated according to equation (1) (left-hand side) and the [001] dislocation dissociated according to equation (2) (right-hand), respectively.

Owing to the symmetry of the (110) plane the direction of $\mathbf{b_2}$ has to be $[1\,\bar{1}0]$ [17] but the direction of $\mathbf{b_1}$ varies from material to material. The vectors $\mathbf{b_1}$ (and thus also $\mathbf{b_2}$ and $\mathbf{b_3}$) are determined by minima of the γ-surface (see e. g. [7]) that has to be calculated for a given alloy using a reliable description of interatomic forces for the specific material; this is at present provided within the density functional theory (DFT) based methods while results of potentials with an empirical input are merely qualitative. In this paper we examine only the potential consequences of such non-crystallographic metastable planar faults and the corresponding character of dislocation splitting while the results for specific alloys will be published elsewhere. In this context we discuss the basic question why dislocations with much longer Burgers vector <111> rather than <001> may mediate the plastic deformation in some B2 systems. For simplicity the isotropic elasticity is employed in the following study of dislocation dissociations. While this analysis is only qualitative, it demonstrates how the type of dislocations mediating

plastic flow in B2 alloys may vary with the form of metastable stacking-fault-like defects and elastic properties of the material.

ANALYSIS OF DISLOCATION DISSOCIATIONS

The most important characteristics of a stacking-fault-like planar defect on the (110) plane are the magnitude of the vector $\mathbf{b_2}$ that measures the deviation of the displacement vector from the crystallographic vector $\frac{1}{2}[1\,\bar{1}\,1]$ and its energy γ. Let us consider the whole range of such displacements, $\mathbf{b_2} = x/2[1\,\bar{1}0]$, where the parameter x varies from 0, for the APB displacement, up to 1, for the displacement ½[001]. We will now analyse the dislocation splitting as a function of two parameters, x, characterising the geometry of the Burgers vectors of partial dislocations, and the quantity $M = \mu a / 4\pi\gamma$ that characterises the material via the shear modulus μ, the lattice constant a and the energy of the metastable stacking-fault-like defect on the (110) plane γ.

The widths of dislocations dissociated according to (1) and (2) are defined by separations, $2s$ and $2r$, respectively, as shown in Fig. 2. In the following we consider only screw orientations of the dislocations **b** and **a** that have lower elastic energy than corresponding edge dislocations with the same Burgers vectors and may have non-planar cores if not dissociated in the (110) plane. In the framework of linear isotropic elasticity [18] the half widths of the dissociations described by equations (1) and (2) are in the units of the lattice constant a

$$\frac{r}{a} = M\frac{1}{2}\left(\frac{1}{2} - \frac{(1-x)^2}{1-\nu}\right) \tag{3}$$

and

$$\frac{s}{a} = M\left(\frac{b_1}{a}2\sqrt{3}\cos\varphi - 3\left(\frac{b_1}{a}\right)^2\left(\cos^2\varphi + \frac{\sin^2\varphi}{1-\nu}\right)\right) \tag{4}$$

where ν is the Poisson ratio, φ the angle between the vector $\mathbf{b_1}$ and the direction $[1\,\bar{1}\,1]$ and b_1 the magnitude of the vector $\mathbf{b_1}$.

The $[1\,\bar{1}\,1]$ and [001] dislocations can be considered as dissociated if the values of r or s are at least positive. Otherwise the dislocation core is compact and possibly spread spatially. Following eqs. (3) and (4) signs of s and r are controlled by the parameter x and the Poisson ratio ν. Let us consider the Poisson ratio to be in the interval 0.2-0.5 that covers a large spectrum of B2 systems. Fig. 3 then shows the range of x and ν for which the splitting of [001] and $[1\,\bar{1}\,1]$ screw dislocations may occur. In this figure ν is depicted on the abscissa and x on the ordinate. The dissociation of the [001] dislocation can take place in the region above the lower line and the dissociation of the $[1\,\bar{1}\,1]$ dislocation below the upper line. It is seen that the [001] screw dislocation can dissociate according to equation (2) only for x sufficiently large, above about 0.4, i.e. in the upper part of the x-ν domain in Fig. 3. On the other hand, $[1\,\bar{1}\,1]$ screw dislocations may dissociate practically in the whole x-ν domain. In both cases the width of the dissociation depends, of course, on the value of M.

The difference between s and r, i.e. the difference of the half widths of the splittings of $[1\,\bar{1}\,1]$ and [001] dislocations, is plotted in Fig. 4 as a contour map showing the lines of constant differences of separations of partial dislocations. It becomes negative in the upper-right corner of this diagram only when the width of splitting of the [001] dislocation is larger than that of the $[1\,\bar{1}\,1]$ dislocation. The difference is positive and large for low values of the deviation x when the dissociation of the $[1\,\bar{1}\,1]$ dislocation will be much wider.

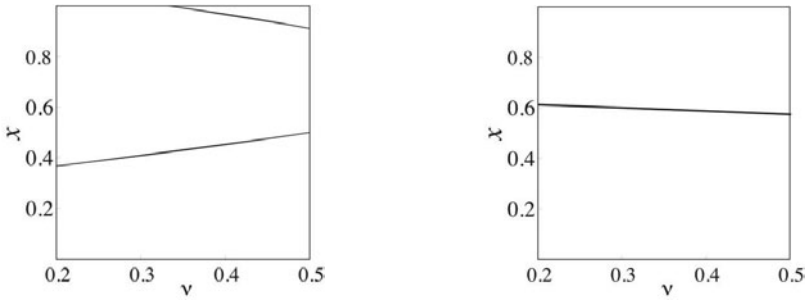

Figure 3. Domains of x and ν in which $[1\,\bar{1}\,1]$ and [001] screw dislocations may dissociate according to equations (1) and (2), respectively. The [001] dislocation may split in the region above the lower line and the $[1\,\bar{1}\,1]$ dislocation below the upper line.

Figure 4. The differences in the width of splittings between the $[1\,\bar{1}\,1]$ and [001] screw dislocations depicted in x - ν plot. Below the line the width of splitting of the $[1\,\bar{1}\,1]$ screw dislocation is by more than 2a larger than that of the [001] screw dislocation.

As mentioned in the introduction, the widely dissociated dislocations are anticipated to be more mobile than the compact ones that may have non-planar cores when in screw orientation. Let us assume that if the width of the splitting of the $[1\,\bar{1}\,1]$ screw dislocation is wider than that of the [001] dislocation by about 2a it is more mobile. In Fig. 4 ν is again depicted on the abscissa and x on the ordinate. In the region below the line the width of splitting of the $[1\,\bar{1}\,1]$ screw dislocation, s, is more than 2a larger than that of the [001] screw dislocation, r, and thus in this region of x and ν the $[1\,\bar{1}\,1]$ screw dislocation is very likely to be more mobile. It is seen from Fig, 5 that this is possible only if $x \leq 0.6$. This is, of course, only a qualitative consideration of the dependence of the width of splitting and thus possibly dislocation mobility on the deviation of the fault vector away from the usually assumed $\frac{1}{2}[1\,\bar{1}\,1]$ APB that will be different for different materials. Moreover, the width of splitting will also depend on the amount of elastic anisotropy. Nevertheless, the present example demonstrates how the differences in mobility of <111> and <001> dislocations may depend on the fact that the metastable planar faults on {110} planes are not necessarily the usually assumed ½<111> APBs.

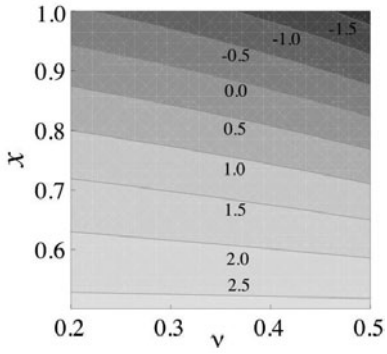

Figure 5. Contour map of constant differences between the half widths *s* and *r* of the splittings of $[1\bar{1}1]$ and [001] screw dislocations. The notation of the contours of the constant difference between *r* and *s* is in units of the lattice parameter *a*.

DISCUSSION

Assuming that the mobility of screw dislocations in B2 alloys depends on their ability to dissociate on {110} planes, we have investigated how this depends on the deviation of the displacements of metastable faults on these planes from the usually assumed vector ½<111>, associated with the {110} APB. This deviation is characterised by the vector $x/2<110>$, where $0 \le x \le 1$. Notice that for $x = 1$ the position of the local minimum of the stacking-fault-like defect would be at the point ½<001> but here any γ-surface exhibits a local maximum [19]. Therefore, very large deviations of the displacement vector away from ½<111> are not likely and thus the region in which the width of splitting of <001> dislocations would be larger that that of <111> dislocations is rather limited (see Fig. 4).

Notwithstanding, in specific materials the widths of dislocation splitting (cores) depend also on material properties enclosed in the present study in the parameter *M*. When it is large, for example because of the low energy of the stacking-fault-like defect, as in CuZn, <111> dislocations will be significantly more split than <001> dislocations, which may not be dissociated at all. On the other hand, when *M* is small, as for example in FeTi, <111> dislocations will be virtually undissociated for any value of *x* and <001> dislocations, albeit also undissociated, will dominate energetically.

In spite of the fact that our analysis provides only a qualitative information on the dissociation of dislocations in B2 alloys, it clearly demonstrates that it is essential to take into account the fact that partial dislocations involved in the splitting of dislocations in these alloys may have Burgers vectors significantly different from the usually assumed ½<111>. A more precise description of dislocation dissociations in specific B2 alloys has to incorporate over and above the considerations of the displacement vectors of stacking-fault-like defects and their energies, the influence of the elastic anisotropy and this will be presented in a forthcoming paper.

CONCLUSIONS

A generic model has been presented that illustrates the effect of the deviation of displacements characterising the metastable planar faults on {101} planes, away from the commonly assumed ½<111> APB, on dislocation behaviour and thus on mechanical properties of B2 intermetallics. The primary consequence is that instead of the two-fold splitting of <111> dislocations, these dissociation may be three-fold, i. e. into three partial dislocations. It has been shown that <001> dislocations are likely to be more widely split than <111> only for large deviations of the fault vectors from ½<111>. However, elastic moduli and energy of the planar faults determine how wide the splitting of <111> dislocations is. In the framework of isotropic elasticity this is controlled by the parameter $M = \mu a / 4\pi\gamma$ that is small for large energies γ.

Hence, if the deviation of the fault vector away from ½<111> is not large and the fault energy γ is small enough the <111> dislocations are widely split and dominate the plastic deformation. The <001> dislocations may dominate either if the deviation of the fault vector from ½<111> is large or when this deviation is not too large but the fault energy γ is so large that the <111> dislocation is undissociated and thus very sessile in the screw orientation (see e. g. [14]). It is, of course, possible that in this case the <001> dislocations are also highly sessile and then the material is brittle since all the screw dislocations are immobile.

ACKNOWLEDGMENTS

This research was supported in part (VP) by the Grant Agency of the Academy of Sciences of the Czech Republic, contract No. IAA100100920, and in part (VV) by the US Department of Energy, BES, Grant no. DEPG02-98ER45702.

REFERENCES

1. T. Takasugi, K. Tsurisaki, O. Izumi and S. Ono, Phil. Mag. A **61** (1990) 785.
2. D. Shindo, M. Yoshida, B. T. Lee, T. Takasugi and K. Hiraga, Intermetallics **3** (1995) 167.
3. J. A. Wollmershauser, C. J. Neil and S. R. Agnew, Met. Mater. Trans. A **41** (2010) 1217.
4. Y. Umakoshi, M. Yamaguchi, Y. Namba and M. Murakami, Acta Metall. **24** (1976) 89.
5. T. Yamagata and H. Yoshida, Mater. Sci. Eng. **12** (1973) 95.
6. D. Wu, I. Baker, P. R. Munroe and E. P. George, Intermetallics **15** (2007) 103.
7. V. Vitek and V. Paidar, in "Dislocations in Solids", edited by J. P. Hirth (North-Holland, Amsterdam, 2008) p. 439.
8. W. A. Rachinger and A. H. Cottrell, Acta Metall. **4** (1956) 109.
9. M. H. Yoo, T. Takasugi, S. Hanada and O. Izumi, Mater. Trans. JIM **31** (1990) 435.
10. T. Takasugi, S. Hanada, M. Yoshida and D. Shindo, Phil. Mag. A **71** (1995) 347.
11. T. A. Parthasarathy, S. I. Rao and D. M. Dimiduk, Phil. Mag. A **67** (1993) 643.
12. D. Farkas, S. J. Zhou, C. Vaihle, B. Mautasa and J. Panova, J. Mater. Res. **12** (1997) 93.
13. C. Vailhe and D. Farkas, Acta Mater. **45** (1997) 4463.
14. R. Schroll, V. Vitek and P. Gumbsch, Acta Mater. **46** (1998) 903.
15. C. Vailhe and D. Farkas, Phil. Mag. A **79** (1999) 921.
16. V. Paidar, Y.-S. Lin, M. Cak and V. Vitek, Intermetallics **18** (2010) 1285.
17. M. Yamaguchi, D. P. Pope, V. Vitek and Y. Umakoshi, Phil. Mag. A **43** (1981) 1265.
18. J. P. Hirth and J. Lothe, Theory of Dislocations (Pergamon, Oxford, 1982).
19. V. Paidar and V. Vitek, in "Intermetalic Compounds, Progress", edited by J. H. Westbrook and R. L. Fleischer (John Wiley, Chichester, 2002) p. 437.

Mater. Res. Soc. Symp. Proc. Vol. 1373 © 2012 Materials Research Society
DOI: 10.1557/opl.2012.289

Exploring the Synthesis Parameters and Spark Plasma Sintering of Tantalum Carbide Powders Prepared by Solvothermal Synthesis

Braeden M. Clark, James P. Kelly, and Olivia A. Graeve*
Kazuo Inamori School of Engineering, Alfred University, Alfred, NY 14802

*Author to whom correspondence should be addressed: Email: graeve@alfred.edu, Tel: (607) 871-2749, Fax: (607) 871-2354, URL: http://people.alfred.edu/~graeve/

ABSTRACT

Tantalum carbide is a technologically important material for use in ultra-high temperatures and corrosive environments. In this report, we describe the scalability of a low temperature solvothermal method for the preparation of this useful material. X-ray diffraction shows phase-pure powders with no change in average crystallite size or compound stoichiometry compared to synthesis in smaller batches, remaining at 25 nm and 0.94 respectively. Dynamic light scattering shows a slight decrease in particle size distribution with scale-up. Thermogravimetric analysis (TGA) in air shows a decrease in surface species on the powders, but the powders oxidize at a lower temperature when scaling the synthesis. Mass spectrometry performed alongside TGA in a helium atmosphere reveals that water is the most abundant species on the surface of the powders, but oxygen, carbon monoxide, carbon dioxide, and nitrogen are also detected. Oxygen analysis reveals that the oxygen content of the powders is high (>6%). The oxygen source and methods of decreasing oxygen content are discussed. Initial sintering trials were performed and demonstrate the need for further powder processing.

INTRODUCTION

Tantalum carbide is of special interest because of its high melting temperature (~4000 K), making it one of the most refractory ceramics known. In addition to being refractory, other properties have been investigated including mechanical strength, oxidation behavior, elasticity, superconductivity, electronic structure, thermodynamic properties and hardness [1-8]. Due to these properties, tantalum carbide is being investigated as a candidate material for use in space reentry vehicles, high Mach aircraft, and propulsion systems, where high temperatures and pressures are sustained.

A novel solvothermal synthesis method has been used to successfully synthesize tantalum carbide and other non-oxide ceramic powders [9-10]. This technique makes use of fused-quartz tubes to allow observation of the reaction; however, this limits the amount of powder that can be synthesized per reaction (~3 g) and risks contamination from the reaction vessel. A scale-up synthesis using the same principles is done in a stainless-steel beaker to reduce contamination and demonstrate scalability of this process.

EXPERIMENTAL PROCEDURE

Reactants for the synthesis were prepared in an argon-filled glove box. The precursors consisted of 92.8 g tantalum (V) chloride (99.8%, Alfa Aesar, Ward Hill, MA) and 9.3 g of carbon (Lampblack 101, Degussa, Parsippany, NJ) and were mixed with a mortar and pestle.

The powders were added to a 600 mL stainless-steel beaker along with 27 g of lithium (granular, 99%, Sigma-Aldrich, St. Louis, MO) and covered with a stainless-steel pan with a weight on top. The reactants were removed from the glove box and placed on a hot-plate inside a chemical fume hood. The hot plate was set at a temperature of 548 K to initiate the self-propagating reaction.

After ignition, the powders were allowed to air cool. The powders were then removed from the beaker by repeatedly adding enough deionized water to submerge the powders and quench the reaction with the excess lithium. The powders and water were added to a beaker and water was added to form a suspension of 1000 mL. The suspension was magnetically stirred for 30 minutes, ultrasonicated for 30 minutes, magnetically stirred for another 15 minutes, centrifuged at 11,000 rpm for 5 minutes, and decanted before washing of the powders.

The washing procedure for the TaC powders consisted of magnetically stirring for 30 minutes, ultrasonicating for 30 minutes, magnetically stirring for another 15 minutes, and centrifuging at 11,000 rpm for enough time to separate the supernatant and powders. The powders were subjected to six of these washes to eliminate excess lithium and then allowed to dry.

The cleaned powders were characterized using X-ray diffraction on a Siemens D5000 instrument scanning from 15° to 85° 2θ with a step size of 0.04° 2θ and a hold time of 1 s. Average crystallite size was determined using the Williamson-Hall technique with Jade 8 software. The lattice parameter was also found, using this software, through unit-cell refinement. The lattice parameters were used to find the compound stoichiometry using the lattice parameter and the relationship C/Ta = 6.398a – 17.516, where a is the lattice parameter [11]. Dynamic light scattering (DLS) via a Nanotrac ULTRA instrument was used to determine the particle size distribution of the powders. The samples were prepared by magnetically stirring 0.01 g of powder in 25 mL of deionized water for 24 hours and then ultrasonicating for 5 minutes before the measurements were taken. Thermogravemetric analysis (TGA) was performed using TA Instruments Q-50 TGA instrument. Weight loss as a function of temperature was measured using a heating rate of 10 K per minute to 1273 K. X-ray photoelectron microscopy (XPS) was performed using a PHI Quantera SXM system from Physical Electronics Inc. Oxygen analysis was performed using a TC600 instrument. Results are compared to a 3 g batch made according to previous work [9-10].

Spark plasma sintering (SPS) was used to sinter TaC specimens on a FCT Systeme D-25 system. Sintering was performed on 6 g samples using a 50 MPa uniaxial pressure and a 100 K/min heating rate to either 1525°C or 1725°C, after which the pressure and current were dismissed and the samples were allowed to cool as quickly as possible. The diameter of the sintered specimens was 1 inch and the thickness was 2-3 mm.

RESULTS AND DISCUSSION

Figure 1 compares the X-ray diffraction patterns of a 3 g batch and a 50 g batch of TaC before and after heat treatment. The results show phase-pure TaC for the 3 g batch whereas a small amount of tantalum metal is observed in the as-synthesized 50 g batch. The tantalum metal reacted after subjecting the powders to heat treatment and was not observed after the heat treatment. The average crystallite size and compound stoichiometry do not show significant changes in the as-synthesized state and are not affected by heat treatments up to 773 K. The average crystallite size was 25 nm for the as-synthesized powders and 26 nm after heat

treatment. The compound stoichiometry was 0.94 C/Ta for powders in the as-synthesized state and 0.94 and 0.93 for the 50 g and 3 g batches, respectively, after heat treatment at 773 K.

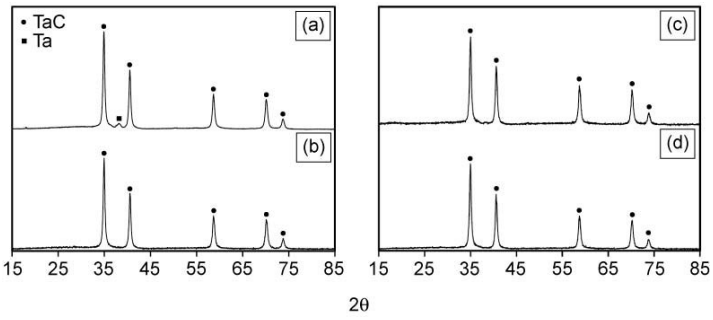

Figure 1. Comparison of X-ray diffraction patterns for (a) as-synthesized 50 g batch, (b) as synthesized 3 g batch, (c) 773 K heat-treated 50 g batch, and (d) 773 K heat-treated 3 g batch.

The particle size distributions for the 3 g batch and the 50 g batch are shown in Figure 2. The average particle size for the 3 g batch was 97 nm, while the average particle size for the 50 g batch was 73 nm. The ratio of average crystallite size to average particle size was reduced from 3.7 to 2.8, indicating lower levels of agglomeration and aggregation when scaling up. Scale-up showed no adverse effects on phase development and it did not cause grain growth or increased agglomeration or aggregation.

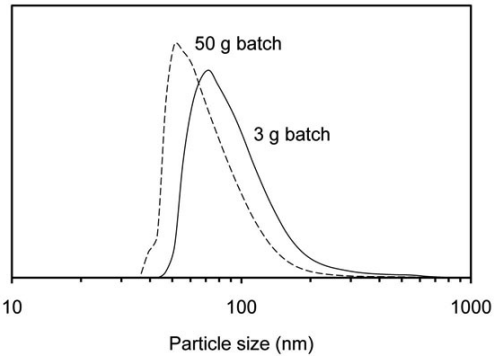

Figure 2. Particle size distributions for the 3 g and 50 g batches of TaC.

XPS spectra of the 3 g and 50 g batch powders are shown in Figure 3. There is little difference in the Ta 4f band, except that the bands were more intense and shifted to slightly

lower binding energies when the synthesis was scaled up. For the 3 g batch, there is a Si 2p band that was observed, indicating contamination from the fused quartz tubes that were used. This peak is not present in the scaled-up batch because a stainless steel reaction vessel was used. Iron could be present in the samples because of the stainless steel container. More definitive evaluation of iron content and removal techniques (if necessary) could be useful. When scaling up, there is a significant increase in the C 1s band area with the appearance of an additional band centered near 288 eV. The increase in the carbon signal is likely related to the increase in tantalum signal and the two are a result of reduced impurities. The O 1s signal has two bands, one centered at approximately 530 eV and the other near 532 eV. In the scaled-up batch, the band at 532 eV was eliminated and is likely a result of transitioning to a stainless steel reaction vessel. The other band centered near 530 eV is not eliminated and could be caused by tantalum oxide, iron oxide, or adsorbed molecules on the surface.

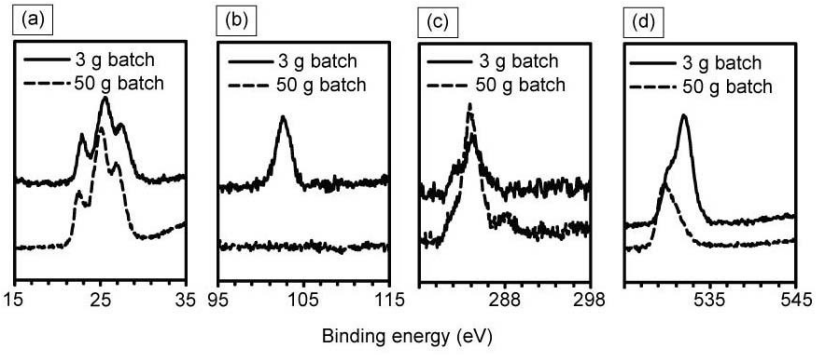

Figure 3. XPS spectra for (a) Ta 4f, (b) Si 2p, (c) C 1s, and (d) O 1s emissions.

TGA of the 3 g batch treated at different temperatures and comparing the effects of scaling are shown in Figure 4. In Figure 4a, it can be seen that the higher the heat treatment temperature, the less adsorbed species on the powders and that heat treatments of at least 600°C were necessary to completely eliminate weight losses. When comparing the two batch sizes in Figure 4b, the 3 g batch has more contaminant in the as-synthesized state than the 50 g batch. The 50 g batch began gaining weight at a lower temperature than the 3 g batch in both the as-synthesized and heat treated state. Results suggest concurrent oxidation and removal of adsorbed species.

The oxygen analysis showed that the oxygen content for the 50 g batch powders was 7.9% in the as-synthesized state. This was reduced to 6.1% on powders heat treated at 873 K for 3 hours in an argon atmosphere. This is a high content for non-oxide powders and can be detrimental to properties.

Figure 5 displays results for the TGA of the 50 g batch of TaC in a helium atmosphere with mass spectrometry. The figure shows that water is the most abundant species on the surface, but oxygen, carbon monoxide, carbon dioxide, and nitrogen are also burned off. The weight loss continues until about 500°C, adding to our previous assessment, oxidation and water removal can occur simultaneously over the temperature range of ~200-500°C. Removing the water from